

AN INVERSE PROBLEM FOR A MODEL OF SCATTERED AND DIFFUSED RADIATION

F. Alberto Grünbaum, Geoff A. Latham and Jorge P. Zubelli

1. INTRODUCTION

There would be many obvious practical applications for any scheme capable of achieving similar goals to, for example, transmission X-ray tomography, but by using instead *low energy* radiation. For example, certain wavelengths of infrared radiation pass easily through human flesh to reveal quite distinct shadow graphs of skeletal structure. Thus diagnostic medical imaging is one possible application. In transmission X-ray tomography, the high energy X-rays travel in essentially straight lines suffering only attenuation, so that the radiation path is known. The immediate problem confronting any attempt at low energy tomography, is that the radiation path is unknown. The low energy radiation is scattered and diffused throughout any body upon which it is incident. Certainly, the radiation paths are not straight lines, or more generally, regularly embedded submanifolds or geodesics for the prevailing metric on the ambient space. This unfortunate fact makes the significant tools of integral geometry, such as the Radon transform which is used with great success for X-rays [3], essentially useless for weak radiation. Conventional mathematical tools having been cast aside, we are forced to take a wider point of view than in classical tomography and construct a first principles model of the radiation-matter interaction.

In this paper, we discuss a discrete model for the passage of low energy radiation through a body, together with the resulting inverse problem coming from trying to reconstruct internal properties of absorption and scattering of the body. We propose a model for the passage of radiation through a discrete lattice of pixels, the radiation being allowed to scatter from the

pixels in only certain fixed directions. The philosophy behind the model, rather than relying heavily on any a priori knowledge of the radiation path, is more in the spirit of Feynman [1,2] in that it tries to incorporate *all* possible radiation paths through the body. It will come as no surprise that any such philosophy when put into a mathematical framework results in a probabilistic description.

In §2 we give the details of the discrete model. Given the physical properties of the body, equations relating the probability of exit at a certain place on the boundary to the absorption and scattering parameters are stated. The forward and inverse problems for our model are formulated in §3. The inverse problem is shown to correspond to the inversion of a nonlinear function. Finally, in §4, we give a number of numerical simulations of reconstructions of the interiors of phantom bodies, using sets of artificially created, and sometimes noisy, external measurements of emitted radiation intensities.

2. THE MODEL

It would be fair to say that at present only discrete schemes seem to offer any hope of success in solving a range of inverse problems associated with low energy radiation scattering. We too follow the well known adage: *Be wise, discretise.*

We begin by covering a body with a two-dimensional square grid (see Fig. 1). This divides the region of the body into n^2 pixels, or sites, which we label with integer cartesian coordinates (i, j) for $1 \leq i, j \leq n$. Around the square grid, we place an array of $4(3n - 1)$ detectors, each capable of measuring the intensity of emitted radiation from the pixel to which it is adjacent. This measurement takes place only in directions which are multiples of 45° and external to the grid (dashed lines in Fig. 1). As in transmission X-ray tomography, the idea is to place a source of intensity one sequentially at each of the $4(3n - 1)$ boundary positions of the grid, and measure the emergent intensity at each detector, for each of the

source positions. We assume for the purposes of describing the model, that radiation is particle like, i.e. composed of photons.

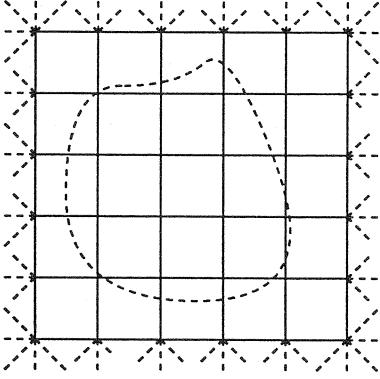


Fig. 1. The physical grid with detectors indicated as dashed lines.

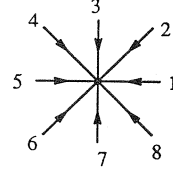


Fig. 2. The convention with directions of approach to pixel (i, j) .

Define the boundary of the grid D by,

$$\partial D = \{(i, j) \mid i = 1, \text{ or } i = n, \text{ or } j = 1, \text{ or } j = n\}.$$

We refer to a pixel on ∂D as an “external” pixel while the rest will be called “internal”. We assume the possible paths of entering or exiting a pixel are confined to one of only eight equally spaced directions (Fig. 2). These directions are numbered 1 through 8 in the sequence shown above. Injected photons undergo a two-dimensional random motion with killing on the lattice D according to the following two rules:

- (i) the photon is absorbed by pixel (i, j) with probability v_{ij} , and so survives a visit to pixel (i, j) with probability $w_{ij} \equiv 1 - v_{ij}$,
- (ii) given that the photon survives at (i, j) , it is scattered in one of the eight possible directions with probabilities, f_{ij} , f_{ij}^l , f_{ij}^r , s_{ij}^l , s_{ij}^r , b_{ij}^l , b_{ij}^r and b_{ij} . The symbols f , s and b stand for forward, side and backward, while the superscripts l and r refer to left and right with respect to the original direction of approach to (i, j) .

To give an example of the convention of scattering probabilities, if a photon entered the pixel (i, j) from direction 1, then it would go in directions 1, 2, 8, 3, 7, 4, 6, 5 with the respective probabilities as listed in (ii). Thus, survival assumed, the probability of being scattered in a certain direction depends only on the angle between the incident and scattered directions. In this sense, a degree of heterogeneity in the scattering properties of a body can be modelled by ‘adjusting’ the scattering probabilities.

It is clear that we must have the condition,

$$f_{ij} + f_{ij}^l + f_{ij}^r + s_{ij}^l + s_{ij}^r + b_{ij}^l + b_{ij}^r + b_{ij} = 1, \quad (1)$$

for $1 \leq i, j \leq n$, since a surviving photon at (i, j) must go somewhere. We now define the main variables of interest in the model. Let,

$P_{ij,\ell}^z =$ the probability of being captured at detector number z

given that the photon entered pixel (i, j) from direction ℓ .

The indexing here runs over, $1 \leq i, j \leq n$, $1 \leq \ell \leq 8$ and $1 \leq z \leq 4(3n - 1)$. The basic equations of the model are the Markov balance equations which relate the $P_{ij,\ell}^z$ to the absorption v_{ij} and the scattering probabilities in (1). The forms of these equations are similar but vary slightly depending on whether the pixel (i, j) in question lies on ∂D or in the interior of D . If the pixel is on the boundary, the forms again vary as to whether it is an “edge” or “corner” pixel of ∂D . We give sample equations for each of these cases.

Interior Pixel: Consider (i, j) to lie in the interior of D . Then we get,

$$\begin{aligned} P_{ij,1}^z = & w_{ij}(b_{ij}P_{i+1,j,5}^z + b_{ij}^rP_{i+1,j+1,6}^z + s_{ij}^rP_{ij+1,7}^z + f_{ij}^rP_{i-1,j+1,8}^z \\ & + f_{ij}P_{i-1,j,1}^z + f_{ij}^lP_{i-1,j-1,2}^z + s_{ij}^lP_{ij-1,3}^z + b_{ij}^lP_{i+1,j-1,4}^z). \end{aligned} \quad (2)$$

Besides this equation, there are seven others corresponding to entering (i, j) from the other seven directions. These equations are simply obtained by ‘cycling’ the scattering probabilities past the variables on the right hand side of (2).

Boundary (edge) Pixel: We consider the edge pixel $(1, j)$, $2 \leq j \leq n-1$ and suppose that the detectors adjacent to this pixel have numbers z_1, z_2 and z_3 going clockwise around ∂D . We then get for example,

$$P_{1j,2}^z = w_{1j}(b_{1j}P_{2j+1,6}^z + b_{1j}^r P_{1j+1,7}^z + s_{1j}^r \delta_{zz_3} + f_{1j}^r \delta_{zz_2} + f_{1j} \delta_{zz_1} + f_{1j}^l P_{1j-1,3}^z + s_{1j}^l P_{2j-1,4}^z + b_{1j}^l P_{2j,5}^z). \quad (3)$$

where δ_{zz_i} is the Kronecker delta. Again there are seven more equations to accompany (3) for the other seven directions of entering pixel $(1, j)$, and these too are obtained by cyclicly permuting the scattering probabilities past the terms on the right hand side of (3).

Boundary (corner) Pixel: Consider the corner pixel $(1, n)$, and let the adjacent detectors be numbered z_1 through z_5 , going clockwise around ∂D . A sample equation for this pixel is,

$$P_{1n,5}^z = w_{1n}(b_{1n} \delta_{zz_2} + b_{1n}^r \delta_{zz_1} + s_{1n}^r P_{1n-1,3}^z + f_{1n}^r P_{2n-1,4}^z + f_{1n} P_{2n,5}^z + f_{1n}^l \delta_{zz_5} + s_{1n}^l \delta_{zz_4} + b_{1n}^l \delta_{zz_3}). \quad (4)$$

Again the other seven equations for $(1, n)$ can be obtained by cycling the scattering probabilities.

Given a pixel $(i, j) \in \partial D$, we define the *external directions* ℓ_e for (i, j) , as the inward pointing directions for that part of ∂D containing (i, j) . For example, all pixels $(1, j) \in \partial D$ which are not corners, have the external directions $\ell_e = 4, 5, 6$. We call the collection

$$\{P_{ij,\ell_e}^z \mid (i, j) \in \partial D, \ell_e \text{ external for } (i, j), z = 1, \dots, 4(3n-1)\},$$

the *external variables* and all the other $P_{ij,\ell}^z$ are called *internal variables*.

For each fixed z , the equations (2), (3), (4) and their companions are linear in the internal and external variables and therefore can be written in the form,

$$\mathbf{A}(\mathbf{w}, \mathbf{f}, \mathbf{s}, \mathbf{b}) \mathbf{p} = \mathbf{d}, \quad (5)$$

where $\mathbf{A} \in M_{8n^2}(\mathbf{R})$, \mathbf{p} and \mathbf{d} are $8n^2$ -vectors, \mathbf{p} with components $P_{ij,\ell}^z$ and the right hand side \mathbf{d} has only a few nonzero components as determined by the detector z under consideration

(see (3) and (4)). We abbreviate the assemblage of absorption and survival probabilities as \mathbf{v} and \mathbf{w} , and the scattering probabilities as \mathbf{f} , \mathbf{s} and \mathbf{b} . Note that each external variable, P_{ij,ℓ_e}^z , can be interpreted as representing the physical quantity which is the intensity of radiation exiting at detector z , given that photons enter the grid from a unit source in the direction ℓ_e at pixel $(i, j) \in \partial D$.

3. THE FORWARD AND INVERSE PROBLEMS

With the model established, we can now state the two problems of interest in this paper. We first state the forward (or direct) problem.

Forward Problem (FP). *Given probabilities w_{ij} , f_{ij} , f_{ij}^l , f_{ij}^r , s_{ij}^l , s_{ij}^r , b_{ij}^l , b_{ij}^r and b_{ij} such that (1) holds, for $1 \leq i, j \leq n$, find all external variables P_{ij,ℓ_e}^z , $(i, j) \in \partial D$ for $z = 1, \dots, 4(3n - 1)$.*

The interpretation of the external variables as emitted intensities means that to solve the FP is equivalent to determining the exit intensities at each detector position for each position of a unit source on the boundary. Put another way, to solve the FP is to find the ‘measured’ emitted intensities given the scattering and absorption properties of the body. Mathematically, this entails solving the system (5) for each of the $4(3n - 1)$ different \mathbf{d} 's corresponding to different detectors, and extracting the external variables from the solution \mathbf{p} .

Of greater interest to us however, is the inverse problem.

Inverse Problem (IP). *Given all the P_{ij,ℓ_e}^z for $(i, j) \in \partial D$, $z = 1, \dots, 4(3n - 1)$, find probabilities w_{ij} , f_{ij} , f_{ij}^l , f_{ij}^r , s_{ij}^l , s_{ij}^r , b_{ij}^l , b_{ij}^r and b_{ij} such that (1) holds, for $1 \leq i, j \leq n$.*

This IP is in the mould of classical tomography. It amounts to: given the external measurements of emitted radiation, find the internal absorption and scattering properties of

a body. Although the forward problem is linear, the inverse problem is highly nonlinear. We reformulate the IP in terms of this nonlinear map.

Denote by

$$\mathbf{M} := \{M_{ij,\ell_e}^z \mid (i, j) \in \partial D, \ell_e \text{ external for } (i, j), z = 1, \dots, 4(3n - 1)\},$$

the ordered set of external measurements (these are just the external variables which we assume are given). It is now of interest to perform a variable count. There are $4n$ boundary pixels surrounded by a total of $4(3n - 1)$ detectors. Likewise, a source can be in any detector position, so there will be a total of $16(3n - 1)^2$ external measurements. For each of the n^2 pixels, there are nine unknowns, one of which is eliminated by the relation (1), leaving a total of $8n^2$ unknowns. Thus in terms of the information available, the IP is, for any reasonable n , well overdetermined. This at least offers heuristic hope that a solution of the IP can be found. Let $\mathbf{P} : \mathbf{R}^{8n^2} \rightarrow \mathbf{R}^{16(3n-1)^2}$ denote the map which takes,

$$(\mathbf{w}, \mathbf{f}, \mathbf{s}, \mathbf{b}) \mapsto \mathbf{M}.$$

Formally, \mathbf{P} might be written as $\Pi \circ \mathbf{A}^{-1}$, where Π is the coordinate projection which selects the external variables from \mathbf{p} . Now the IP is equivalent to inverting the map \mathbf{P} , i.e. solving the nonlinear equations,

$$\mathbf{P}(\mathbf{w}, \mathbf{f}, \mathbf{s}, \mathbf{b}) = \mathbf{M}. \tag{6}$$

The size and complexity of the equations represented by (6) prohibit an analytic solution except when n is very small, e.g. $n = 1, 2$. Even the power of modern symbolic computation balks at the task. We are therefore forced to resort to numerical methods. To solve (6), we employ a constrained nonlinear least squares minimization algorithm to find,

$$\min \|\mathbf{P}(\mathbf{w}, \mathbf{f}, \mathbf{s}, \mathbf{b}) - \mathbf{M}\|_2^2 \tag{7}$$

where the minimization is done over the physical set of variables \mathbf{w} , \mathbf{f} , \mathbf{s} and \mathbf{b} , which must all lie between 0 and 1 and satisfy (1). The advantage of a simple least squares approach is that packaged software is already available to solve this part of the problem. However, using standard algorithms, we are faced with the unpleasant prospect of being trapped in one of many local minima in performing (7).

It is worthwhile mentioning several variations of the IP as stated above. It is possible for example, to *fix* one or more of the scattering probabilities at every pixel, and try to solve (6) only for the remaining ones as well as the absorption v_{ij} . An interesting case of this is to fix $f_{ij}^l = f_{ij}^r = b_{ij}^l = b_{ij}^r = 0$. In this case, the number of scattering directions at every pixel is reduced to only four. Another variation might be to fix the ‘left’ and ‘right’ parameters to be always equal, thus creating two fold symmetry in the problem. If on the other hand, we make $f_{ij} = s_{ij}^l = s_{ij}^r = b_{ij} = 0$, then the forward and inverse problems decouple onto two distinct square lattices, with $\mathbf{A} = \mathbf{A}_1 \oplus \mathbf{A}_2$ for a suitable ordering of the variables. Many other variations are also possible. It is possible to derive interesting scaling results for arbitrarily large n for some of these simplified models [5,6].

4. SOME NUMERICAL EXPERIMENTS

In this section, we give some examples of reconstructions of scattering and absorption properties based on the solution of (6) via (7). Performing the minimization (7) is fairly computationally intensive. The main reason for this is the need to solve the system (5) for each evaluation of \mathbf{P} . Thus any method using finite differences to perform a gradient minimization will spend a lot of time in the solution of linear systems. Of course, the gradient of \mathbf{P} could be calculated, but this would again involve the solution of a linear system.

To obtain our measurements \mathbf{M} , we proceed as follows. We first construct a *phantom* object by choosing a sufficiently interesting set of absorption and scattering parameters \mathbf{v} , \mathbf{f} ,

\mathbf{s} and \mathbf{b} . Next the FP is solved to produce the external variables P_{ij,ℓ_e}^z , $(i, j) \in \partial D$, which we then rename the external measurements M_{ij,ℓ_e}^z . With this artificial data, we attempt to solve (6) by employing a variation of the Levenberg–Marquardt algorithm [7], beginning from an initial guess \mathbf{w}_0 , \mathbf{f}_0 , \mathbf{s}_0 and \mathbf{b}_0 , usually chosen to be uniform in (i, j) . In the examples below, the effect of adding noise to the external measurements is also considered. This is done by instead of taking the exact values of M_{ij,ℓ_e}^z , we take a perturbation of them by varying amounts of white noise, and then try to reconstruct the actual parameters \mathbf{v} , \mathbf{f} , \mathbf{s} and \mathbf{b} . Our aim in doing this is to give some indication of the noise level needed to cause a breakdown of the reconstruction.

We consider two forms of the IP: first, the full problem of reconstructing \mathbf{v} , \mathbf{f} , \mathbf{s} and \mathbf{b} (Fig. 3), and second, the variation in which the scattering probabilities \mathbf{f} , \mathbf{s} and \mathbf{b} are fixed, and only a reconstruction of \mathbf{v} is sought (Figs. 4–6). Our two-dimensional reconstructions are presented in the form of density plots. The square at location (i, j) in the density plot is assigned a grey scale value according to the value of the plotted variable at the corresponding pixel of the physical grid. Darker shades correspond to smaller values and lighter shades to larger values. We prefer to plot \mathbf{w} instead of \mathbf{v} so that highly absorbing regions appear darker. In plots of \mathbf{f} , \mathbf{s} , \mathbf{b} however, the reverse is true with larger scattering probabilities appearing as lighter grey scales. Because of the computationally intensive nature of our inverse problem, we restrict the examples to be merely of illustrative size, which in practical terms means low resolution (small n). All the examples below were computed in single precision.

Fig. 3 shows the result of the solution of the IP for a forward scattering phantom on a 4×4 grid. Each row of the figure gives a reconstruction with a different amount of noise. The zero noise reconstruction (first row) is indistinguishable from the phantom itself, and so the phantom is not plotted. Even at 5 and 10% noise levels, major features of the phantom

are discernable, but considerable degradation has also taken place.

Figs. 4–6 show reconstructions for w_{ij} (equivalently v_{ij}) only, the scattering probabilities having been fixed. Both Figs. 4 and 5 show good immunity to noise, perhaps with Fig. 4 doing slightly better than Fig. 5. Fig. 6 is however, a noiseless reconstruction, and yet shows some difference compared to the phantom (probably due to the use of only single precision). Notice the artifacts in the central region and the slight difference in shading of objects there.

Although we have shown only successful reconstructions, it is not difficult to design sufficiently complex phantoms or choose a sufficiently poor initial guess, for which the reconstruction algorithm fails completely.

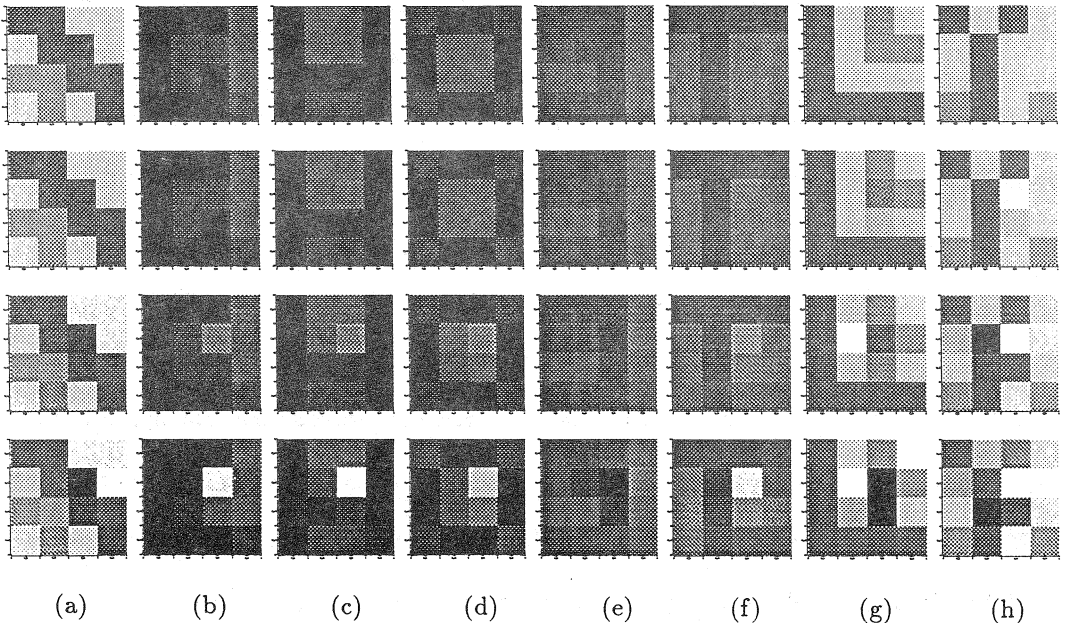


Fig. 3. Full reconstruction of a 4×4 phantom with no noise (first row) 1% noise (second row) 5% noise (third row) and 10% noise (last row). The columns from left to right are plots of (a) w_{ij} , (b) f_{ij} , (c) f_{ij}^l , (d) f_{ij}^r , (e) s_{ij}^l , (f) s_{ij}^r , (g) b_{ij}^l and (h) b_{ij}^r respectively. The starting point for the reconstruction was, $w_{ij} = 0.7$, $f_{ij} = f_{ij}^l = f_{ij}^r = 0.2$, $s_{ij}^l = s_{ij}^r = 0.1$ and $b_{ij}^l = b_{ij}^r = 0.03$. The values for the phantom vary in the ranges, $w_{ij} \in [0.5, 0.9]$, $f_{ij} \in [0.20, 0.24]$, $f_{ij}^l, f_{ij}^r \in [0.15, 0.20]$, $s_{ij}^l, s_{ij}^r \in [0.10, 0.13]$ and $b_{ij}^l, b_{ij}^r \in [0.02, 0.04]$.

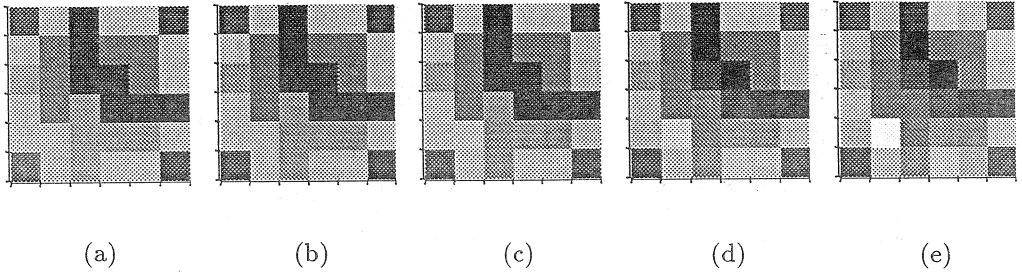


Fig. 4. Reconstructions of w only for the 6×6 phantom in (a), with (b) no noise, (c) 1% noise, (d) 5% noise and (e) 10% noise. All reconstructions were done with a starting value of $w_{ij} = 0.7$ and scattering probabilities fixed at $f_{ij} = 0.24$, $f_{ij}^l = 0.19$, $f_{ij}^r = 0.21$, $s_{ij}^l = 0.13$, $s_{ij}^r = 0.17$, $b_{ij}^l = 0.02$, $b_{ij}^r = 0.03$ and $b_{ij} = 0.01$. The phantom's values vary in the range $w_{ij} \in [0.5, 0.9]$.

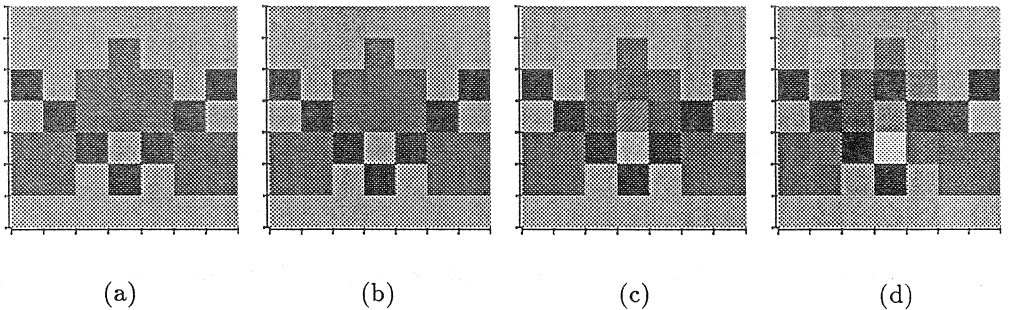


Fig. 5. Reconstructions of w only for the 7×7 phantom in (a) with (b) no noise, (c) 1% noise and (d) 5% noise. Each reconstruction had a starting point of $w_{ij} = 0.8$ and scattering probabilities were fixed at $f_{ij} = 0.24$, $f_{ij}^l = f_{ij}^r = 0.20$, $s_{ij}^l = s_{ij}^r = 0.15$, $b_{ij}^l = b_{ij}^r = 0.025$ and $b_{ij} = 0.01$. The phantom's values vary in the range $w_{ij} \in [0.56, 0.91]$.

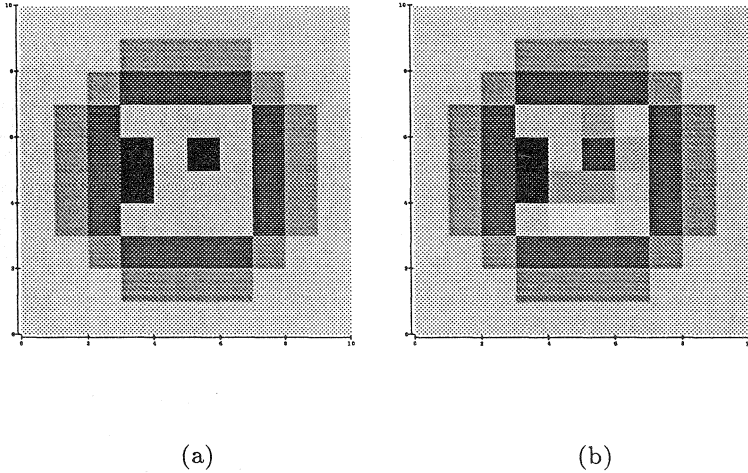


Fig. 6. A noiseless reconstruction of w for the 10×10 phantom in (a) is shown in (b). The starting point was $w_{ij} = 0.9$ and the scattering probabilities were fixed at, $f_{ij} = 0.24$, $f_{ij}^l = f_{ij}^r = 0.20$, $s_{ij}^l = s_{ij}^r = 0.15$, $b_{ij}^l = b_{ij}^r = 0.025$ and $b_{ij} = 0.01$. The phantom's range of values was $w_{ij} \in [0.46, 0.94]$.

5. CONCLUDING REMARKS

Although in this paper we have concentrated on a two-dimensional square grid, it is easy to extend the model to other grids and higher dimensions. In this regard, reference [4] contains an implementation of a similar model on a three-dimensional square grid. The only problem in going to a triangular or hexagonal grid, or indeed more exotic tilings, is that the book keeping for internal and external variables becomes more troublesome.

Of greater concern for possible applications however, are, the large computational effort required to attain a reasonable resolution, and the question as to whether the model itself

is applicable to any real world radiation–matter interaction. Both of these problems may be avoided by instead of inventing a first principles model, taking a well established transport equation and discretizing that equation. For this approach, the possibility of using multi-level methods offers the promise of greatly increased speed. Another advantage may be that some of the problems caused by local minima can be lessened or removed. Other exotic computational methods may also be of use. These are some of the directions of our current work.

REFERENCES

- [1] R.P. Feynman, *QED: the strange theory of light and matter*, Princeton University Press, 1985.
- [2] R.P. Feynman and A.R. Hibbs, *Quantum mechanics and path integrals*, McGraw–Hill, New York, 1965.
- [3] F. Natterer, *The mathematics of computerized tomography*, Tuebner–Wiley, Stuttgart, 1986.
- [4] J.R. Singer, F.A. Grünbaum, P. Kohn and J.P. Zubelli, Image reconstruction of the interior of bodies that diffuse radiation, *Science* **248** (1990), 990–993.
- [5] F.A. Grünbaum, Relating microscopic and macroscopic parameters for a 3-dimensional random walk, *Comm. Math. Phys.* **129** (1990), 95–102.
- [6] F.A. Grünbaum, Renormalization of exit probabilities and a theorem of Poincaré, *Physics Lett. A* **146** (1990), 486–491.
- [7] Å. Björck, Solution of equations in \mathbf{R}^n (Part I): Least squares methods, in P.G. Ciarlet and J.L. Lions (general editors), *Handbook of Numerical Analysis Vol I*, North–Holland Elsevier, New York, 1990.

Department of Mathematics, University of California, Berkeley, CA 94720 USA
 Centre for Mathematical Analysis, Australian National University, GPO Box 4, Canberra
 ACT 2601 Australia
 Department of Mathematics, University of California, Santa Cruz, CA 95060 USA